Particle Stimulated Nucleation in Coarse-Grained Ferritic Stainless Steel

RODRIGO PINTO DE SIQUEIRA, HUGO RICARDO ZSCHOMMLER SANDIM, and DIERK RAABE

Particle-stimulated nucleation (PSN) is investigated in Nb-containing ferritic stainless steel. Coarse-grained sheets were cold rolled to 80 pct thickness reduction and annealed from 973 K to 998 K (700 °C to 725 °C) to obtain partially recrystallized microstructures. Electron backscatter diffraction was performed around coarse niobium carbonitride particles (larger than 1 μm) within coarse grains (~1 mm), with different host orientations in both deformed and annealed states. In the deformed state, the deformation zones around both spherical and rectangular particles were investigated. The local lattice rotations about the transverse direction necessary to accommodate the particle-matrix strain incompatibility were observed in all grains investigated. After annealing, recrystallization occurs preferentially around coarse particles at the initial stages of recrystallization. Based on a total number of 130 grains nucleated *via* PSN, we observe both, randomly oriented and minor $\{111\}\langle 110\rangle$ oriented texture components. The results also reveal that PSN in this material is not associated with a specific host orientation.

DOI: 10.1007/s11661-012-1408-x

I. INTRODUCTION

IT is well known that dispersed non-deformable particles affect both deformed and recrystallized microstructures of several relevant industrial materials such as steels and aluminum alloys.[1–5] The term "*non-deformable*" means that particles are elastically stiff and much harder than matrix acting as obstacles to dislocation motion. Dislocations are able to bypass these particles and the nature of the dislocation structure developed around non-deformable particles is almost independent of particle mechanical properties.[6] Remarkable changes in the microstructure and crystallographic texture were reported to depend mainly on particle dispersion parameters such as particle volume fraction, size, shape, and interparticle spacing.[7] During large strain deformation of materials containing coarse particles, *i.e.*, with sizes larger than 0.1 μm,[8] non-deformable particles can induce a high degree of local lattice curvature in their vicinity due to the particle-matrix strain incompatibility and, consequently, more complex dislocation structures are formed.[3,8] These regions are in the literature referred to as *deformation zones*.[9] During subsequent annealing, such particle-related deformation zones are favorable nucleation sites for primary recrystallization and this mechanism is, hence, referred to as particle-stimulated nucleation (PSN).[3]

Most of the literature on the nature of deformation zones is focused on particle-containing face-centered cubic (fcc) materials.[2,10–16] Several works in fcc particle-containing polycrystalline alloys have shown that new grains that nucleated around particles are randomly oriented.[11,17–21] Starting from single-crystal materials, the orientations of the new grains were found to be related to the host orientation of the deformed crystal in which the inhomogeneous deformation zone was formed.[22–24] Recent investigations regarding the effects of non-deformable particles on the nature of the deformation zone were also performed in intermetallic materials such as Fe_3Al alloys with B2 ordered structure.[13,25–27] A new approach referred to 3D high-resolution EBSD has been used to characterize deformation zones in Ni[24,28] and Fe_3Al-based alloys.[29]

In spite of the great industrial importance of carbon and ferritic stainless steels (FSS), PSN mechanism is much less investigated in body-centered cubic (bcc) materials. The effect of spherical cementite particles on the nature of the deformation zone has been studied by Gawne and Higgins[30] in a cold-rolled Fe-0.4 pct C alloy. They found that, although the particle size was only 0.6 μm, large misorientations formed in the deformation zones and PSN occurred in these areas randomizing the recrystallization texture. Similar results were also reported by Dillamore *et al.*[31] in heavily compressed Fe-C alloys. Regarding corresponding phenomena associated with more complex particle morphologies, Inagaki investigated the effect of lamellar cementite on the development of the cold-rolling texture using transmission electron microscopy (TEM).[2] In his work complex deformation zones were observed around the fragmented cementite particles. It was found that the spread of

RODRIGO PINTO DE SIQUEIRA, PostDoc, and HUGO RICARDO ZSCHOMMLER SANDIM, Associate Professor, are with the Departamento de Engenharia de Materiais, Escola de Engenharia de Lorena, Universidade de São Paulo, Lorena SP, 12600-970 Brazil. Contact e-mail: hsandim@demar.eel.usp.br DIERK RAABE, Professor, is with the Max-Planck Institut für Eisenforschung (MPIE), 40237 Düsseldorf, Germany.

Manuscript submitted September 29, 2011.
Article published online September 18, 2012

orientations around cementite particles during deformation lead to a decrease in the strength of the rolling texture.

In the present work, we investigate PSN in Nb-containing 16 wt pct Cr FSS (AISI 430; 1.4016; X6Cr17). This steel has good corrosion resistance and good cold formability.[32–35] An important technological reason for studying PSN effects in FSS is that these materials commonly reveal ridging and roping phenomena during stretching and related forming operations.[36,37] The surface undulations have been shown to be related to the frequently occurring large non-recrystallized {001}⟨110⟩-oriented grain clusters that are often inherited from the hot band through cold rolling and incomplete recrystallization into the final sheets. PSN is hence anticipated to promote more homogeneous recrystallization of these materials and the break-up of these texture components. The fully ferritic microstructure contains coarse dispersed Nb-rich particles.[35] Various types of Nb-rich precipitates such as Nb(C,N), Fe_2Nb and Fe_3Nb_3C were reported in Nb-containing FSS, depending on their respective compositions and aging conditions. According to experimental data (X-ray diffraction) and thermodynamic calculations reported in the literature, only Nb(C,N) particles are expected to be found in the FSS used in the present investigation.[38,39] During cold rolling, the microstructural subdivision varies from grain to grain, as reported earlier to take place in other coarse-grained bcc materials.[40,41] This orientation split-up effect was individually investigated within coarse grains. The orientation gradients were determined in terms of crystal lattice rotations in the vicinity of the particles (deformation zones) within large grains with different initial host orientations with aid of automated electron backscatter diffraction (EBSD) in the scanning electron microscope. After annealing, the texture components associated with PSN grains were also evaluated.

II. EXPERIMENTAL

The 4-mm thick Nb-containing FSS hot bands with a composition of 16.22 pct Cr, 0.37 pct Nb, 0.02 pct C, 0.02 pct N, 0.15 pct Mn, 0.30 pct Si, 0.03 pct P (in wt pct) were supplied by Aperam S.A. (Brazil). Specimens were annealed in argon atmosphere at 1523 K (1250 °C) for 2 hours followed by air cooling to obtain large grains (mm-range) which are suitable to investigate orientation effects during deformation and further static annealing. A detailed description of the microstructure and texture of the coarse-grained Nb-containing FSS used in this work is given elsewhere.[42] The volume fraction of niobium carbonitride particles was found to be less than 0.01.[43] After hot band annealing, these specimens were cold rolled (near plane strain condition) resulting in a sheet of 0.8 mm thickness (80 pct engineering thickness reduction, true strain $\varepsilon = 1.6$) and annealed in argon atmosphere at temperatures varying from 973 K to 998 K (700 °C to 725 °C) for 15 minutes in order to achieve a partially recrystallized microstructure appropriate to study the PSN mechanism. Microtextural characterization was carried out in the longitudinal plane using EBSD. The metallographic preparation was carried out with 800, 1200 and 2400 grit SiC abrasive papers with water followed by fine grinding with 3-μm diamond suspension. The final polishing step was performed with a colloidal silica suspension. The orientation maps were performed in a JEOL JSM-6500F field emission gun scanning electron microscope (FEG-SEM) operating at 15 kV. A map step size of 50 nm was used. EBSD data were evaluated using the EDAX-TSL software package and displayed using inverse pole figure (IPF) maps. The non-indexed black areas indicated in the IPF maps appear at the locations of coarse Nb(C,N) particles which do not produce an electron diffraction pattern. The black and white lines mark high-angle (>15 deg misorientation) and low-angle boundaries (<15 deg misorientation), respectively, in all IPF maps. The {011} pole figures and [001] IPFs were determined *via* discrete-binning from the EBSD data.

III. RESULTS AND DISCUSSION

A. *Deformed State*

The cold-rolled microtextures for distinct large grains were characterized by EBSD using IPF maps (Figures 1, 2, 3, 4, 5, and 6). Different regions in the microstructure surrounding coarse Nb(C,N) particles were marked and respective crystal lattice rotations are shown in the discrete {011} pole figures. The orientation maps of two different grains with orientations close to 45 deg ND-rotated cube are shown in Figures 1 and 2, respectively. These grains were chosen because they have very stable orientations belonging to the α fiber (the α-fiber refers to all orientations with a common ⟨110⟩ axis along the rolling direction RD). The IPF maps show in detail the presence of deformation zones around coarse Nb(C,N) particles. In the first IPF map, a spherical coarse particle located in the center of the 45 deg ND-rotated-cube grain can be observed (Figure 1(a)). The regions 1 and 2 around the particle display a few low angle grain boundaries. The orientation distribution in regions 1 and 2 (Figures 1(c) through (d)) is quite similar to the matrix orientation (particle-free regions, Figure 1(b)). However, in region 3, the crystal rotates about the TD reaching an orientation close to $(111)[11\bar{2}]$, as shown in Figure 1(e). This deformation zone around the particle lies parallel to the RD. The misorientation between the matrix in region 1 and the deformation zone in region 3 is about 45 deg. In the second IPF map, a cluster of coarse particles is located close to the grain boundary region (Figure 2(a)). Three regions belonging to 45 deg ND-rotated-cube grain (1 to 3) were marked in the IPF map (Figure 2(a)). The deformation zones are also elongated in the RD, as shown in region 3. The {011} pole figures corresponding to regions 1, 2 and 3, respectively, show that these regions exhibit different orientations (Figures 2(b) through (d)). The results have shown that this deformation zone also rotates about the TD towards to the orientation $(\bar{1}\bar{1}1)[213]$ (rounded by up to 10 deg misorientation from these ideal texture

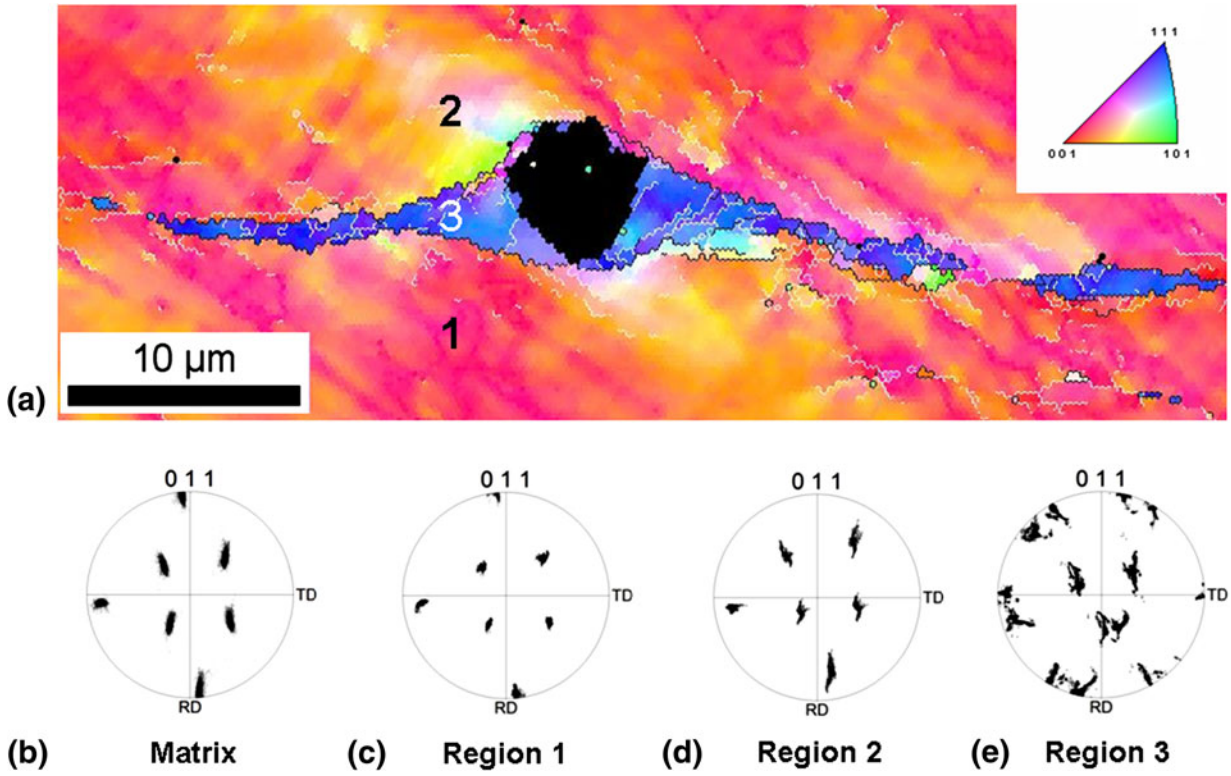

Fig. 1—EBSD results showing the deformation heterogeneity nucleated around a spherical particle (black in the map) in the center of a 45 deg rotated-cube large grain: (*a*) IPF map; (*b*) {011} pole figure of the large grain; (*c*) through (*e*) {011} pole figures corresponding to the regions 1, 2, and 3, respectively.

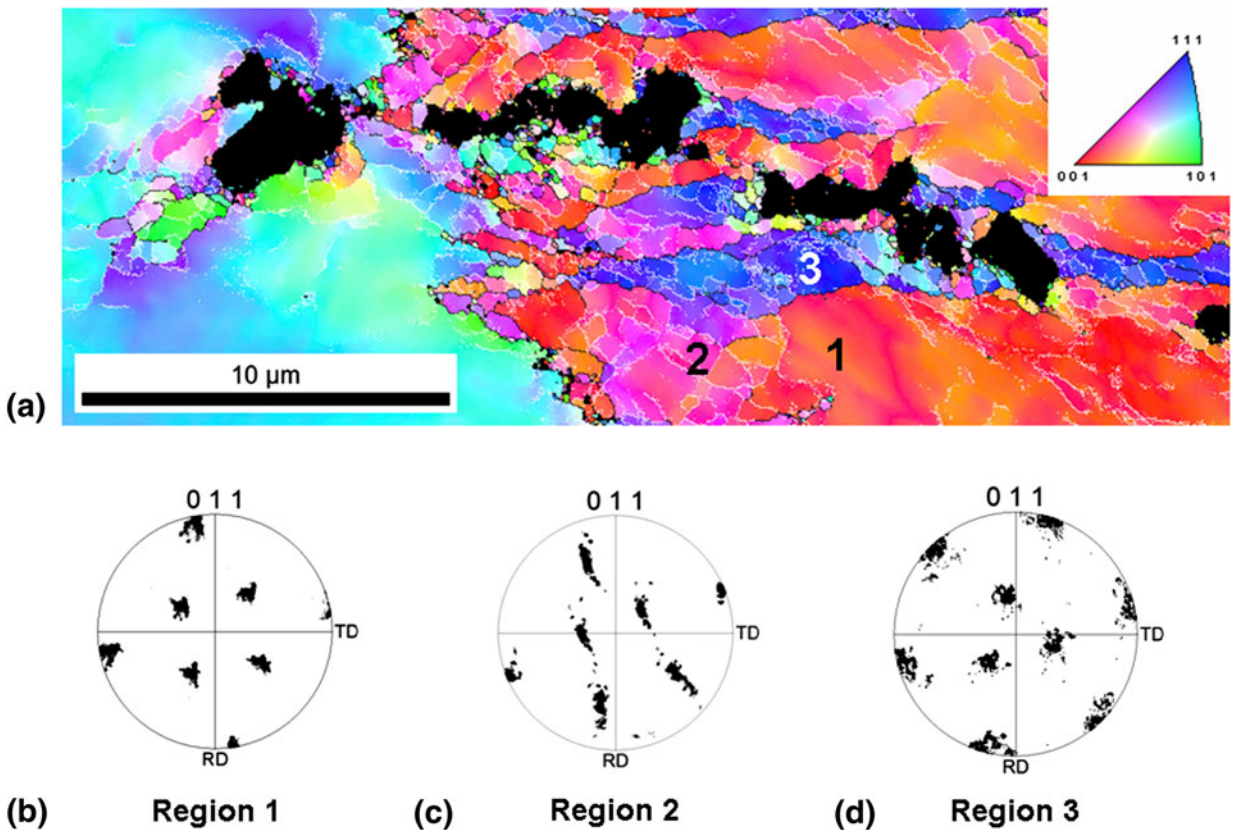

Fig. 2—EBSD results showing the deformation heterogeneity nucleated around a cluster of particles (black in the map) in the grain boundary region of a 45 deg rotated-cube large grain: (*a*) IPF map; (*b*) through (*d*) {011} pole figures corresponding to the regions 1, 2, and, 3, respectively.

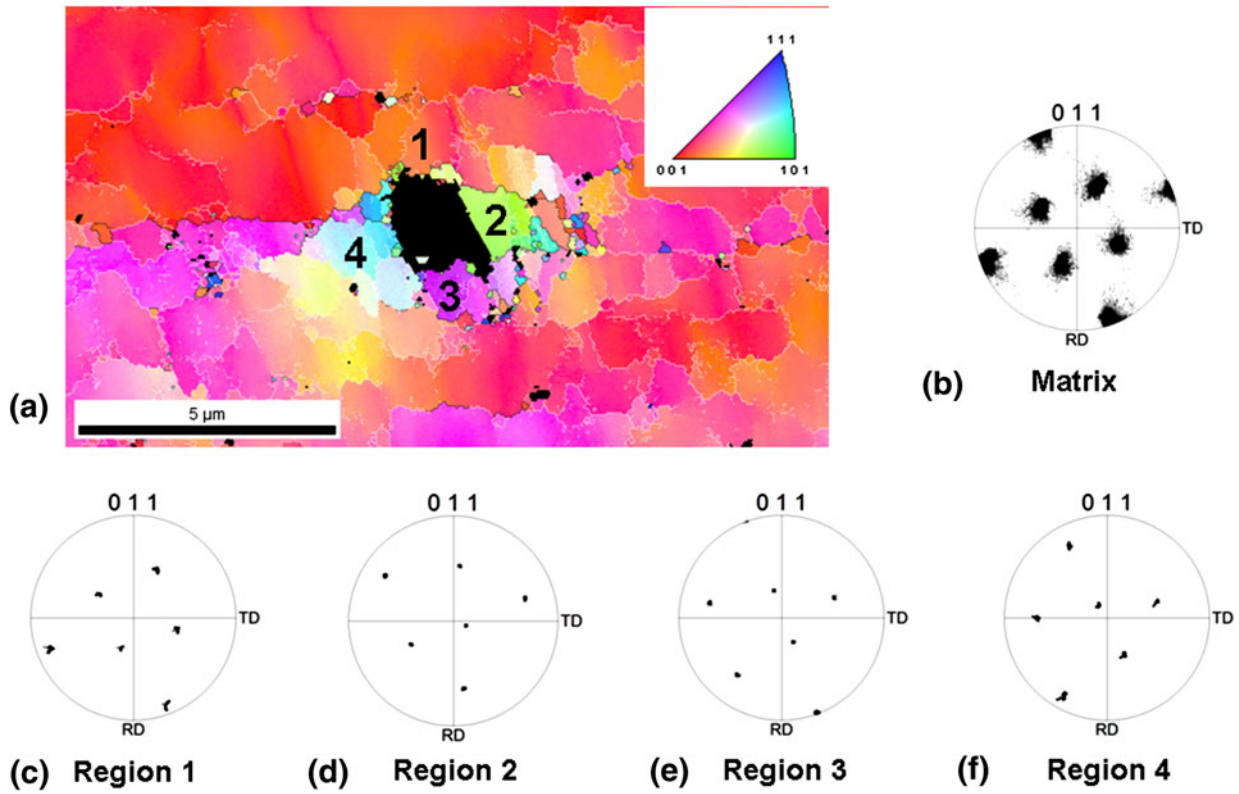

Fig. 3—EBSD results showing four distinct deformation zones around a coarse particle (black in the map) within a (001)[210] large grain: (*a*) IPF map; (*b*) {011} pole figure of the particle-free matrix and (*c*) through (*f*) {011} pole figures corresponding to the regions 1, 2, 3 and 4, respectively.

components). In Figure 3(a), the deformation zone in a large grain with orientation (001){210] (Figure 3(b)) can be observed. In this case, the presence of a single coarse particle induced local lattice rotations in the deformation zone (regions 1 to 4, as shown in Figure 3(a)). Their orientations are displayed in the pole figures in Figures 3(c) through (f). The results reveal that these regions are rotated about the TD. The misorientation angles in regions 2, 3 and 4 (end point) with respect to region 1 (point of origin) are 35, 41 and 45 deg, respectively. Deviations from TD were observed (>15 deg about the ND) for region 2, whereas regions 3 and 4 rotate only about the TD.

Coarse grains belonging to the γ fiber were also mapped. The γ fiber refers to all grains with a common $\langle 111 \rangle$ axis parallel to the sheet normal. Figure 4(a) shows a $(\bar{1}11)[1\bar{2}3]$-oriented grain where deformation zones around three coarse particles are observed. The matrix (region 1) is quite fragmented with several low angle boundaries (white lines). This fragmentation is in line with theoretical predictions of grain stability of $\{111\}\langle uvw \rangle$ oriented crystals.[44] In the deformation zones (regions 2 and 3), high angle boundaries (black lines) are visible indicating a large degree of fragmentation. The orientation of the regions adjacent to the particle rotates significantly about the TD towards an end orientation close to $(001)[1\bar{1}0]$ (Figures 4(c) and (d)). The misorientation angles in regions 2 and 3 (end points) with respect to the region 1 (point of origin) are 55 and 47 deg, respectively. In Figure 5 it is possible to observe the same local lattice rotation about the TD occurring in the corner of a coarse cuboidal particle within a $(3\bar{2}2)[011]$-oriented grain. The orientation in the rotated region is close to $(1\bar{1}0)[\bar{1}\bar{1}2]$. The deformation zone around another particle with elongated morphology within the same host grain shown in Figure 5 was also investigated. The lattice rotation about the TD is clearly visible in the corners of the particle (Figure 6). Table I summarizes the main results of the EBSD characterization where point-to-origin rotations were determined starting from more remote regions of the deformed matrix (about 10 μm far away from particles) to areas within the deformation zone.

The aforementioned results clearly show that the local lattice rotation about the TD in the deformation zone occurs in all investigated matrix orientations (both, in α- and γ-fiber grains). In all cases the particle size is larger than 1 μm. These results suggest that particle size is not the predominant effect for this size range (about 1 to 5 μm). Further lattice rotations about the ND or the RD (deviations from the TD) were not frequently observed. Many preceding studies have reported rotations about the TD in the deformation zones.[9,11,12,15,16,25] The local lattice rotation is necessary to accommodate the particle-matrix strain incompatibility under global plane-strain conditions. A detailed discussion about the thermodynamics of the lattice rotation around non-deformable particles is

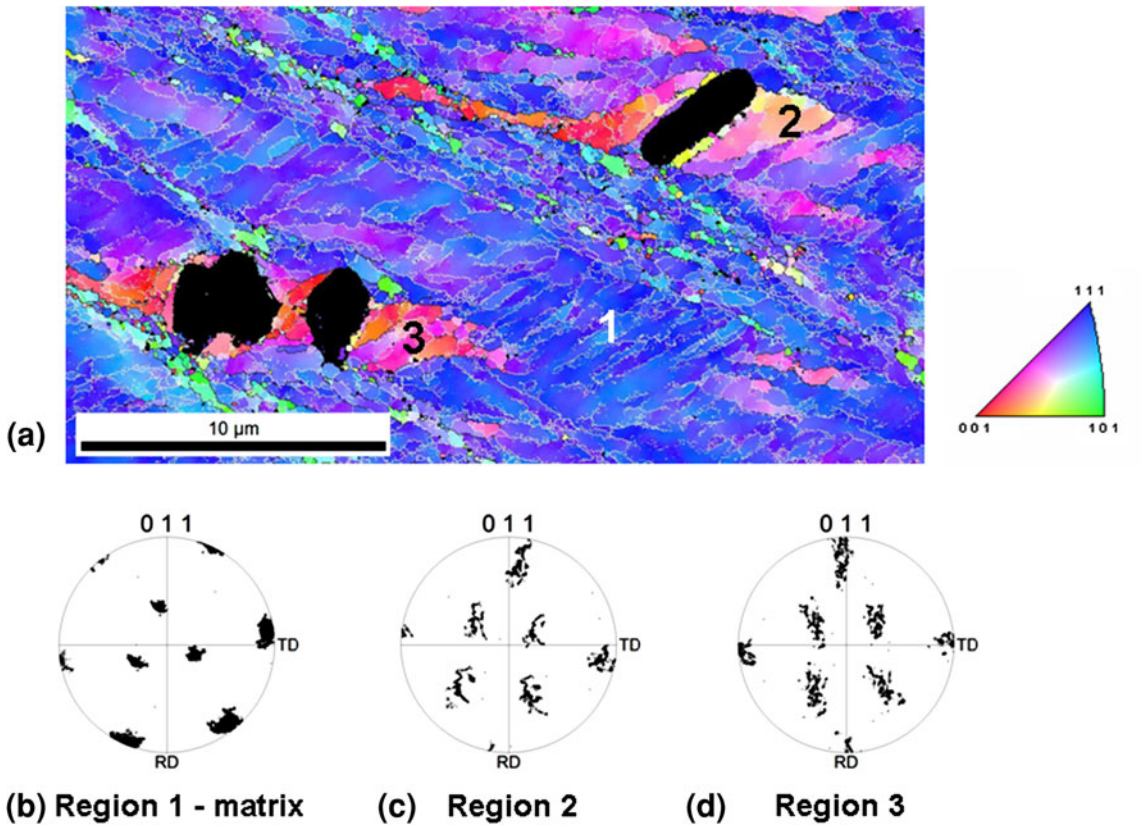

Fig. 4—EBSD results showing the distinct deformation zones around three particles (black in the map) within a γ-fiber large grain: (*a*) IPF map; (*b*) through (*d*) {011} pole figures corresponding to the regions 1, 2, and 3 respectively.

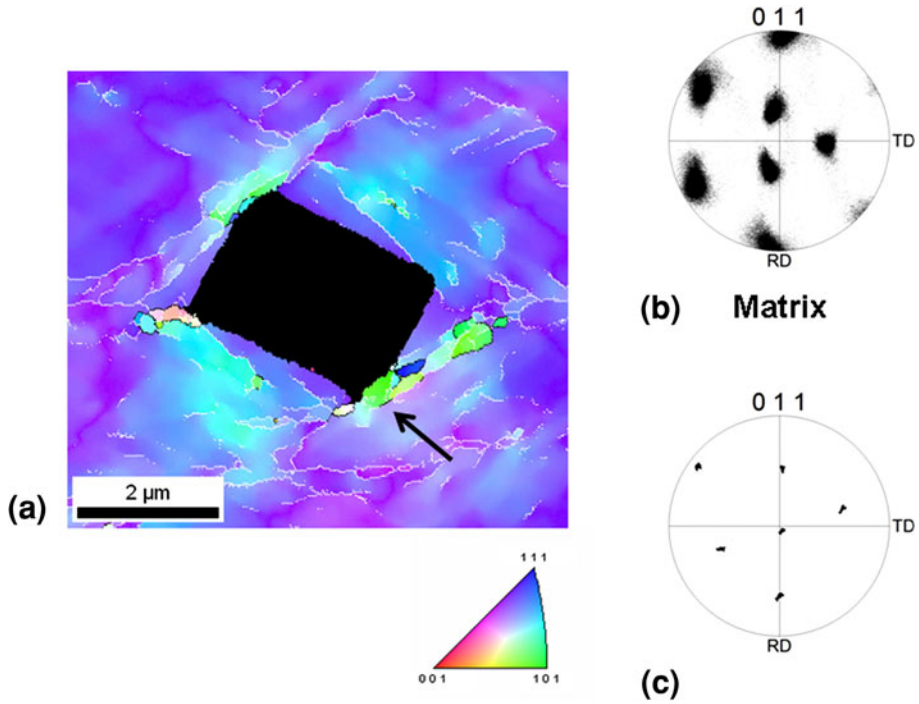

Fig. 5—EBSD results showing the deformation zone around a rectangular particle (black in the map): (*a*) IPF map; (*b*) {011} pole figure of the particle-free matrix and (*c*) {011} pole figure corresponding to the corner of the large particle (indicating by arrow).

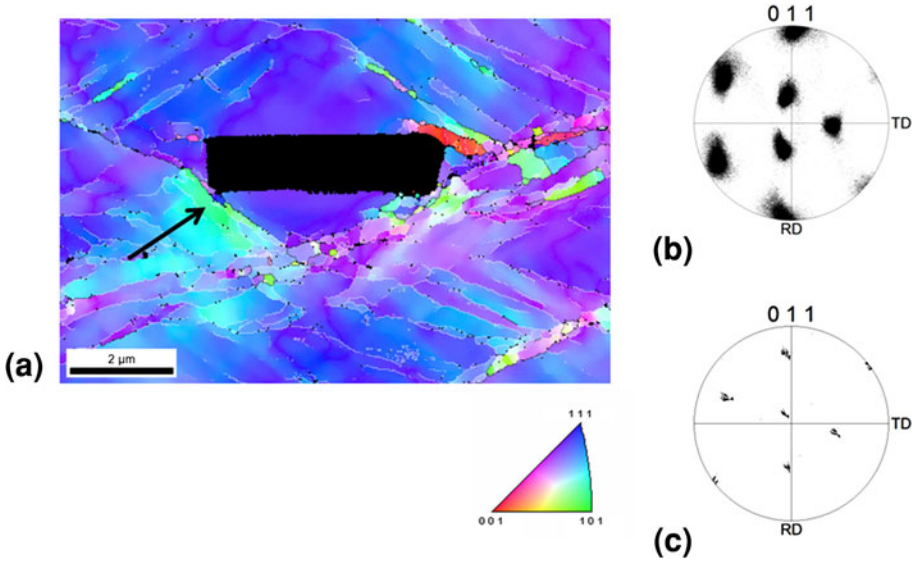

Fig. 6—EBSD results showing the deformation zone around an elongated particle (black in the map): (*a*) IPF map; (*b*) {011} pole figure of the particle-free matrix and (*c*) pole figure corresponding to the corner of the large particle (indicating by arrow).

Table I. Point-To-Origin Rotations Corresponding to the Grains Shown in Figs. 1, 2, 3, 4, 5, and 6

Figure	Deformed Matrix	Deformation Zone	Maximum Misorientation (Degrees)
1	(001)[110]	(111)[112]	≈45
2	(001)[110]	(111)[213]	≈55
3	(001)[210]	(365)[559]	≈45
4	(111)[123]	(001)[110]	≈55
5	(322)[011]	(110)[112]	≈30
6	(322)[011]	(101)[121]	≈30

presented by Schäfer *et al.*[12] In their finite element model (FEM) model, it is assumed that the sum of the energies of the geometrically necessary dislocations (GNDs) and the Taylor energy for plastic deformation needs to be minimized to define the required local amount of relaxation and local slip activity. The microtexture within the deformation zone developed around spherical and cuboidal particles was modeled in detail by means of a Taylor type deformation texture model using strain path data from finite element predictions for a global plain strain compression path.[12] Recently, Kobayashi *et al.*[13] reported that the presence of non-deformable particles within the 45 deg ND-rotated-cube orientation changes the plane-strain deformation field promoting a favorable condition for shear at the vicinity of the particle. This new deformation mode leads to the activation of slip system combinations resulting in the local lattice rotation about the TD.

The results also show that depending on the shape of the particles (*e.g.*, spherical or rectangular), different misorientation build up takes place around the particle during deformation (see Figures 1 and 5). Our results are in reasonable agreement with simulations of the strain path around non-deformable particles with different shapes reported by Schäfer *et al.*[12] Computer-based simulations also showed that particle shape has a strong effect on both the number and the spatial distribution of potential recrystallization nuclei in the deformation zone.[45] The simulations have also shown that the deformation zone developed around spherical particles extends significantly along to the forward direction of the deformation (flow material direction; in rolling processes equivalent to the RD) rather than into the perpendicular directions (ND and TD). This feature is clearly visible in Figure 1. The maximum equivalent plastic strain was found about 45 deg to the forward direction in the particle-matrix interface. Regarding particles with a rectangular shape, the maximum equivalent plastic strain is observed around the corners of the particle. These regions experience high total strains that lead to large local lattice rotations in the deformation zone. Similar results like those shown in Figures 5 and 6 were also observed in Fe_3Al alloys. In this case, large local lattice rotations are preferentially found at the tips of elongated rod-like κ-Fe_3AlC precipitates in grains with a 45 deg ND-rotated-cube host orientation. The maximum local misorientation angles between the particle-affected zones on the one hand and the more remote in-grain zones on the other reach values as large as 45–60°.[13,27] Therefore, our results confirm that the particle shape seems to affect the misorientation build up in the deformation zone.

B. *Annealed State*

The occurrence of PSN mechanism at the early stages of recrystallization is shown in Figures 7 and 8. The color code used in the IPF maps is associated with the orientations shown in both the pole figures and the IPFs (Figures 9 and 10). The deformed matrix corresponding

to a coarse 45 deg rotated-cube-oriented grain is predominantly recovered. However PSN grains are clearly observed (dash-square) in Figure 7. It is well-known that coarse grains with 45 deg ND-rotated-cube orientation in bcc metals commonly deform homogeneously during cold rolling (near plane-strain condition) developing a structureless microstructure and potential recrystallization nuclei generally are absent even after long recrystallization annealing.[40,46,47] Nevertheless, the presence of non-deformable particles in this otherwise very stable crystal orientation leads to the development of large local lattice rotations in the deformation zone. As discussed above, shear occurs around particles instead of the globally imposed near plane-strain condition. This deviation from the plane-strain boundary conditions leads to the development of local orientation instabilities. After annealing, these highly-misoriented regions act as favorable nucleation sites for recrystallization even in this otherwise stable host orientation.

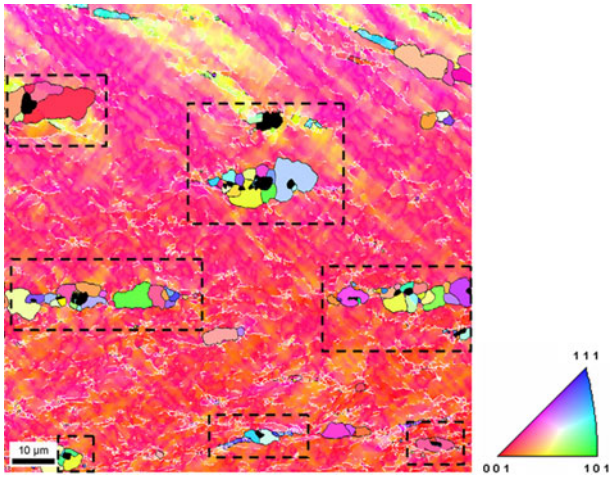

Fig. 7—IPF map showing recrystallized grains (dash square) nucleated preferentially around particles (black in the map) in a 45 deg rotated-cube large grain cold rolled and further annealed at 998 K (725 °C) for 15 min.

The individual orientations of about 60 individual grains that were formed *via* the PSN mechanism in a coarse grain belonging to the α-fiber was determined as shown in Figure 9(b). The orientation spread observed in the corresponding {011} pole figure suggests that grains formed by PSN are randomly oriented. This is a time-consuming experiment since large areas have to be mapped due to the large interparticle spacing found in this steel (50 to 100 μm).

In another coarse host grain with $(1\bar{1}2)[110]$ orientation (Figure 8), three distinct regions showing PSN grains were mapped. In this large host grain, recrystallization was incomplete and the new recrystallized grains can also be explained in terms of the PSN mechanism. The crystallographic orientations of about 70 grains formed *via* the PSN mechanism were determined as shown in Figure 10(b). Regarding the orientation spread observed in the {011} pole figure, the PSN grains are also randomly oriented, such as observed for the α-fiber host grain discussed above. It is worth mentioning

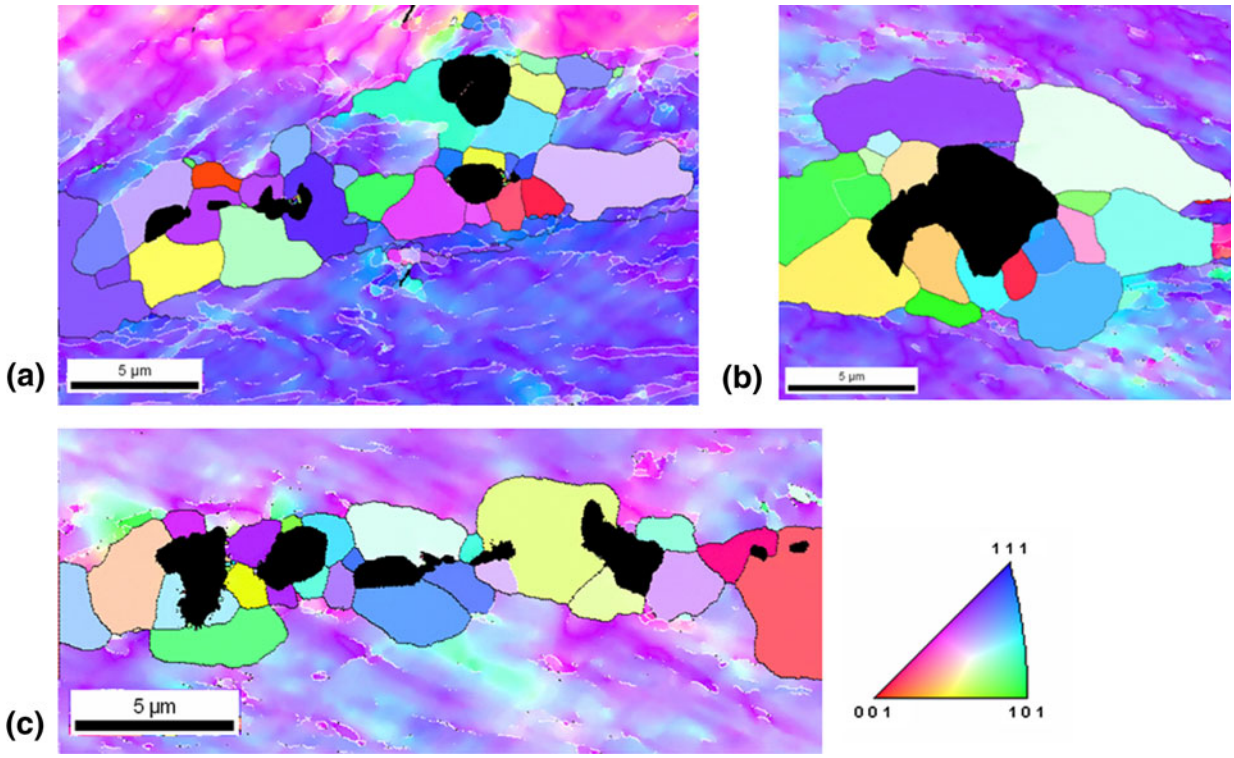

Fig. 8—IPF maps (*a*) through (*c*) showing recrystallized grains nucleated preferentially around particles (black in the map) in a (112)[110] large grain cold rolled and further annealed at 988 K (715 °C) for 15 min.

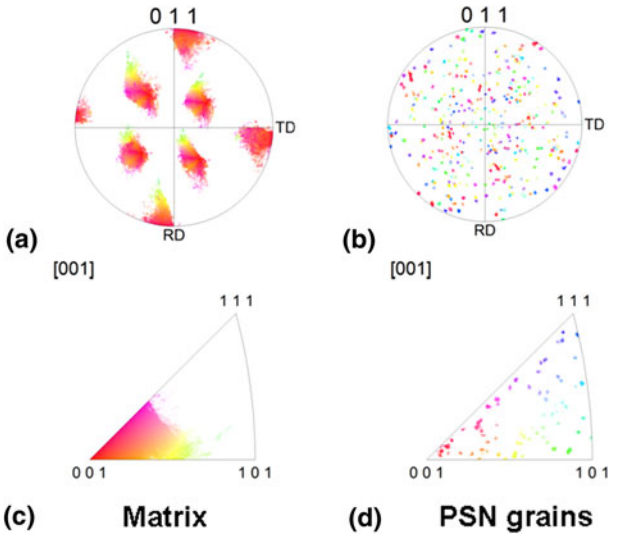

Fig. 9—The {011} pole figures and [001] IPFs of the partially recrystallized microstructure displayed in the IPF map in Fig. 7: (*a*) through (*c*) matrix large grain (recovery region); (*b*) through (*d*) PSN grains.

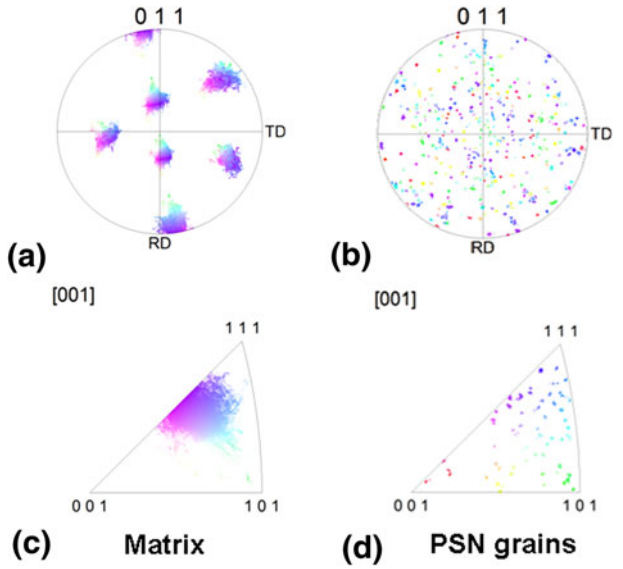

Fig. 10—The {011} pole figures and [001] IPFs of the partially recrystallized microstructure displayed in all IPF maps in Fig. 8: (*a*) through (*c*) matrix large grain (recovery region); (*b*) through (*d*) PSN grains.

that in both cases a small portion of the PSN-formed grains has orientations close to those of the respective deformed host matrix surrounding them, as shown in Figures 9(c) and (d) and 10(c) and (d). Based on the limited number of PSN grains investigated (about 130 PSN grains), it is not possible neither including nor excluding the presence of the $\{111\}\langle 110\rangle$ component in an unequivocally manner.

The relationship between the deformation zones and the orientations of the nuclei formed in the PSN-affected region has been investigated before in particle-containing fcc structured alloys. Several authors reported that the PSN nuclei orientations have similar crystallographic orientations to those observed inside the deformation zones of Al[10,24] and Ni[18] single crystals. According to these results, however, the PSN nuclei seem to be randomly oriented in polycrystalline metals because of the orientation spread developed around particles increasing the number of potential recrystallization nuclei. Our results show indeed that different orientations appear in the annealed material due to the PSN mechanism. Therefore, the new grains formed *via* the PSN mechanism are efficient in minimizing the ridging and roping phenomena during stretching and related forming operations in FSS. Their inherent orientation spread is large enough to destabilize specifically the α-fiber grains. Since particularly the large 45 deg ND-rotated-cube grains form clusters that usually display only partial recrystallization, the new grains that are formed *via* PSN contribute to a change in the global texture and particularly in the clustering of such orientations. PSN hence promotes grain refinement, texture randomization, and the reduction in texture clustering in this steels. On the other hand, in the $\{111\}$ γ-fiber grains, the grains nucleated *via* PSN can contribute to an increase in the random texture components so that the γ-fiber texture tends to be less intense.

Regarding bcc metals, the results in the literature suggest that randomly oriented grains nucleated *via* PSN appear after recrystallization annealing in deformed polycrystals.[25,26] Inagaki reported the development of complex microstructures around to fragmented cementite particles in low-carbon steels after cold rolling.[2] During annealing of theses steels with different amounts of carbon, the influence of PSN on the recrystallization kinetics, especially at low annealing temperatures was investigated. It is reported that PSN-grains resulting from slow heating of deformed samples leads to oriented growth of the $\{111\}\langle 110\rangle$ components.[48] As a result, randomly oriented grains should nucleate from inside the deformation zones suppressing the development of a strong $\{111\}$ γ-fiber texture. The results reported by Gawne and Higgins[30] using spherical cementite particles in steels also support this statement. In a recent paper, De Cock *et al.*[49] reported the effect of the PSN nuclei in the static recrystallization of the cold-rolled low-carbon steels. According to the authors, the orientation of the recrystallized PSN grains contributes to an increase in the random texture component. They also confirm that the γ-fiber texture was less intense in such cases.

To a certain extent, the coarse-grained material investigated herein has characteristics of both single crystals and polycrystalline materials. Isolated particles surrounded by large volumes of deformed material might be compared to the scenario found in PSN in deformed single crystals. Experiments on single crystals show that the PSN nuclei are not randomly oriented whereas random texture is associated with PSN grains during recrystallization of polycrystals, as summarized by Humphreys and Hatherly.[8] Based on a total number of 130 grains nucleated *via* PSN mechanism within different host grain orientations, we observe both,

randomly oriented and minor $\{111\}\langle 110\rangle$ oriented texture components. This particular microstructure, *i.e.*, a low volume fraction of coarse particles embedded in coarse grains, might explain the results of texture of PSN grains found in our study.

IV. CONCLUSIONS

Particle stimulated nucleation (PSN) has been investigated in coarse-grained Nb-bearing FSS with aid of EBSD. The most important findings of the present investigation are the following:

1. Coarse non-deformable niobium carbonitride particles with sizes larger than 1 μm play an important role during the nucleation of recrystallized grains in 80 pct cold-rolled Nb-bearing FSS steel.
2. During cold deformation, the local lattice rotation about the TD axis in the deformation zone surrounding the particles seems to be necessary to accommodate the particle-matrix strain incompatibility. Our results suggest that this crystal lattice rotation about the TD does not depend on the starting orientations.
3. The development of deformation zones around coarse particles depends significantly on the particle morphology. Different particle shapes, *e.g.*, spherical or rectangular, can induce distinctly strain paths in the vicinity of the particle during deformation.
4. After annealing, new PSN grains are found around particles at the initial stages of recrystallization. Based on a total number of 130 PSN grains investigated, we observe both, randomly oriented and minor $\{111\}\langle 110\rangle$ oriented texture components.
5. The results show that PSN is an effective nucleation mechanism for recrystallization even in otherwise stable orientations such as the 45 deg ND rotated cube component in bcc grains.

ACKNOWLEDGMENTS

The authors acknowledge Brazilian research funding agencies FAPESP (Grant no. 05/60131-5) and CNPq for providing financial support for this work. We also thank Dr. T. R. Oliveira (Aperam S.A, Brazil) for supplying the steel used in the investigation. The kind assistance of Mrs. Katja Angenendt (MPI-E, Düsseldorf) in both metallographic preparation and EBSD sessions is deeply acknowledged.

REFERENCES

1. C. Kamma and E. Hornbogen: *J. Mater. Sci.*, 1976, vol. 11, pp. 2340–44.
2. H. Inagaki: *Z. Metall.*, 1987, vol. 78, pp. 630–38.
3. F.J. Humphreys: *Acta Metall.*, 1977, vol. 25, pp. 1323–44.
4. F.J. Humphreys: *Acta Mater.*, 1979, vol. 27, pp. 1801–14.
5. O. Engler, J. Hirsch, and K. Lücke: *Acta Metall. Mater.*, 1995, vol. 43, pp. 121–38.
6. R.E. Smallman and R.J. Bishop: *Modern Physical Metallurgy and Materials Engineering*, 6th ed., Butterworth-Heinemann, Oxford, 1999, p. 265.
7. H. Mecking and G. Gottstein: *Recrystallization of Metallic Materials*, Dr. Riederer-Verlag, Stuttgart, 1978, p. 170.
8. F.J. Humphreys and M. Hatherly: *Recrystallization and Related Annealing Phenomena*, 2nd ed., Elsevier, Oxford, 2004, p. 285.
9. F.J. Humphreys: *Mater. Sci. Forum*, 2004, vols. 467–470, pp. 107–16.
10. F.J. Humphreys and M.G. Ardakani: *Acta Metall. Mater.*, 1994, vol. 42, pp. 749–61.
11. O. Engler: *Scripta Mater.*, 1997, vol. 37, pp. 1675–83.
12. C. Schäfer, J. Song, and G. Gottstein: *Acta Mater.*, 2009, vol. 57, pp. 1026–34.
13. S. Kobayashi, C. Zambaldi, and D. Raabe: *Acta Mater.*, 2010, vol. 58, pp. 6672–84.
14. M. Ferry and F.J. Humphreys: *Acta Mater.*, 1996, vol. 44, pp. 3089–3103.
15. O. Engler, X.W. Kong, and P. Yang: *Scripta Mater.*, 1997, vol. 37, pp. 1665–74.
16. Q. Liu, Z. Yao, A. Godfrey, and W.J. Liu: *J. Alloys Compd.*, 2009, vol. 482, pp. 264–71.
17. O. Engler, P. Yang, and X.W. Kong: *Acta Mater.*, 1996, vol. 44, pp. 3349–69.
18. O Engler, HE Vatne, and E Nes: *Mater. Sci. Eng. A*, 1996, vol. 205, pp. 187–98.
19. H.M. Chan and F.J. Humphreys: *Acta Metall.*, 1984, vol. 32, pp. 235–43.
20. F.J. Humphreys: *Acta Mater.*, 1997, vol. 45, pp. 5031–39.
21. W.D. Hutchinson and H. Homma: *Proceedings of 3rd International Conference on Grain Growth*, H. Weiland, B.L. Adams and A.D. Rollett, eds., TMS, Pittsburgh, PA, 1998, p. 387.
22. M.G. Ardakani and F.J. Humphreys: *Acta Mater.*, 1994, vol. 42, pp. 763–80.
23. M. Ferry and F.J. Humphreys: *Acta Mater.*, 1996, vol. 44, pp. 1293–1308.
24. F.J. Humphreys: *Scripta Mater.*, 2000, vol. 43, pp. 591–96.
25. S. Kobayashi, S. Zaefferer, A. Schneider, D. Raabe, and G. Frommeyer: *Intermetallics*, 2005, vol. 13, pp. 1296–1303.
26. S. Kobayashi, A. Schneider, S. Zaefferer, G. Frommeyer, and D. Raabe: *Acta Mater.*, 2005, vol. 53, pp. 3961–70.
27. D. Raabe and W. Mao: *Phil. Mag. A*, 1995, vol. 71, pp. 805–13.
28. W. Xu, M. Ferry, J.M. Cairney, and F.J. Humphreys: *Acta Mater.*, 2007, vol. 55, pp. 5157–67.
29. J. Konrad, S. Zaefferer, and D. Raabe: *Acta Mater.*, 2006, vol. 54, pp. 1369–80.
30. D.T. Gawne and G.T. Higgins: *Textures in Research and Practice*, J. Grewen and G. Wasserman, eds., Springer, New York, 1969, p. 369.
31. I.L. Dillamore, H. Katoh, and K. Haslam: *Texture*, 1974, vol. 1, pp. 151–56.
32. Steel Heat Treatment: *Metallurgy and Technologies*, CRC Press, Boca Raton, FL, 2007, p. 695.
33. *ASM Metals Reference Book*, ASM, Materials Park, OH, 1993, p. 112.
34. *Steel Products Manual*, Iron and Steel Society, Warrendale, PA, 1999, p. 251.
35. M. Hölscher, D. Raabe, and K. Lücke: *Steel Res.*, 1991, vol. 62, pp. 567–75.
36. M.-Y. Huh, J.-H. Lee, S.H. Park, O. Engler, and D. Raabe: *Steel Res.*, 2005, vol. 76, pp. 797–806.
37. M.Y. Huh and O. Engler: *Mater. Sci. Eng. A*, 2001, vol. 308, pp. 74–87.
38. G.M. Sim, J.C. Ahm, S.C. Hong, K.J. Lee, and K.S. Lee: *Mater. Sci. Eng. A*, 2005, vol. 396, pp. 159–65.
39. N. Fujita, M. Kikuchi, and K. Ohmura: *ISIJ Int.*, 2003, vol. 43, pp. 1999–2006.
40. N. Tsuji, K. Tsuzaki, and T. Maki: *ISIJ Int.*, 1992, vol. 32, pp. 1319–28.
41. H.R.Z. Sandim and D. Raabe: *Scripta Mater.*, 2005, vol. 53, pp. 207–12.
42. R.P. Siqueira, H.R.Z. Sandim, and T.R. Oliveira: *Mater. Sci. Eng. A*, 2008, vol. 497, pp. 216–23.

43. R.P. Siqueira: Ph.D. Thesis. University of Sao Paulo, Lorena, SP, 2010.
44. D. Raabe, Z. Zhao, S.-J. Park, and F. Roters: *Acta Mater*., 2002, vol. 50, pp. 421–40.
45. B. Radhakrishnan and G. Sarma: *Philos. Mag*., 2004, vol. 84, pp. 2341–66.
46. D. Raabe and K. Lücke: *Scripta Metall*., 1992, vol. 27, pp. 1533–38.
47. D. Raabe: *Steel Research*, 1995, vol. 66, pp. 222–29.
48. H. Inagaki: *Z. Metall*., 1991, vol. 82, pp. 99–107.
49. T. De Cock, C. Capdevila, F.G. Caballero, and C.G. Andrés: *Mater. Sci. Eng. A*, 2009, vol. 519, pp. 9–18.